Evaluation of a photon-counting breast tomosynthesis imaging system

Andrew Maidment[a], Michael Albert[a], Stefan Thunberg[b], Leif Adelöw[b], Ola Blom[b], Johan Egerström[b], Mathias Eklund[b], Tom Francke[b], Ulf Jordung[b], Tomas Kristoffersson[b], Karin Lindman[b], Lars Lindqvist[b], Daniel Marchal[b], Hans Olla[b], Erik Penton[b], Juha Rantanen[b], Skiff Solokov[b], Christer Ullberg[b], Niclas Weber[b]

a) University of Pennsylvania, Philadelphia PA, USA
b) XCounter AB, Svärdsvägen 11, SE-182 33 Danderyd, Sweden

ABSTRACT

Digital breast tomosynthesis promises solutions to many of the problems currently associated with projection mammography, including elimination of artifactual densities due to the superposition of normal tissues and increasing the conspicuity of true lesions that would otherwise be masked by superimposed normal tissue. We have investigated tomosynthesis using 45 photon counting, orientation sensitive, linear detectors which are precisely aligned with the focal spot of the x-ray source. The x-ray source and the digital detectors are scanned in a continuous motion across the object (patient); each linear detector collecting an image at a distinct angle. Simulations of the imaging system were performed to evaluate the effect of: (1) the range of angles over which projection images are acquired; and (2) the number of projection images acquired used in the tomosynthetic reconstruction. Two different simulations were evaluated; the first was a numerical simulation of a tungsten wire; the second consisted of tomosynthetic reconstructions of a cadaveric rabbit, in which the number and/or range of projection angles was varied. We have shown, analytically and through these simulations, that both the use of more projection angles and the use of a larger range of projection angles improve the image quality of tomosynthetic image reconstructions. The use of a photon-counting x-ray detector system allows us to consider image acquisition geometries with a large number of projection angles, as there is no additive detector noise to degrade the projection or reconstructed images. The maximum number of projection angles and the range of projections angles do have upper practical limits; the range of projection angles is determined predominantly by the detector element size.

Keywords: Digital breast tomosynthesis, synthetic tomography, digital mammography

1. INTRODUCTION

Projection mammography is subject to a number of fundamental limitations related to the projection process, whereby two-dimensional images are produced of the three-dimensional breast anatomy. First, mammograms can produce artifactual densities from the superposition of normal tissues that are separated in space; although only visible in a single view, these are often sufficiently suspicious in appearance to necessitate a biopsy, leading to a loss in specificity.[1] In addition, however, true lesions in mammograms can be masked by superimposed normal tissue and thereby render the lesion invisible; this reduces the sensitivity of mammography.[1] Tomosynthesis, a three-dimensional technique for imaging the breast, has the potential of mitigating both limitations, while also providing a simple means of localizing lesions in three-dimensions.[2,3]

We have investigated tomosynthesis using a prototype XC Mammo -3T digital synthetic tomography breast imaging system (Xcounter, Danderyd, Sweden). The system incorporates an x-ray camera consisting of 45 photon counting, orientation sensitive, linear detectors which are precisely aligned with the focal spot of the x-ray source. The x-ray source and the camera are scanned in a continuous motion across the object (patient), each linear detector collecting an image at a distinct angle. The collected images are of a very high image quality due to several special characteristics of this detector technology.[4,5] First, the detectors are insensitive to scattered radiation; the detector geometry ensures that only primary photons emanating from the focal spot of the x-ray source will elicit a response from the detector. Second,

Medical Imaging 2005: Physics of Medical Imaging, edited by Michael J. Flynn,
Proceedings of SPIE Vol. 5745 (SPIE, Bellingham, WA, 2005)
1605-7422/05/$15 · doi: 10.1117/12.597317

the detector does not contribute any electronic noise; the strong gaseous amplification of each photon interaction allows a simple threshold to exclude electronic noise from being counted and included in the final image. Finally, the detector technology does not have any residual image, ghosting or blooming artifacts.

Digital breast tomosynthesis is a new and developing field; as such, there are many factors that may ultimately affect image quality which have not yet been adequately explored. We have sought both qualitative and quantitative means by which to model system performance and to optimize system design. In this paper, we have examined the role of the total angular range and number of projection angles used in the tomosynthesis image reconstruction, and the detector element (del) size. For the same total dose to the breast, increasing the number of angles necessarily decreases the signal recorded per projection angle. Thus, in most systems, detector noise limits the maximum number of angles that can be acquired. As will be shown in this paper, the XC Mammo -3T photon-counting detector technology does not introduce any detector noise, and thus does not limit the number of projection angles which can be acquired. We have utilized this property and source (projection) images acquired with the prototype system to simulate various imaging geometries.

2. METHODS AND MATERIALS

Simulations of the imaging system were performed to evaluate the effect of: (1) the range of angles over which projection images are acquired; and (2) the number of projection images used in the tomosynthetic reconstruction. Two different simulations were evaluated; the first was a numerical simulation of a tungsten wire; the second consisted of tomosynthetic reconstructions of a cadaveric rabbit, in which the number and/or range of projection angles was varied.

2.1. Tungsten Wire Simulation

An attempt was made to quantitatively evaluate the image quality of various image reconstruction geometries. The specific geometries are detailed in tables 1 and 2. In each case, projection images of a 25 μm tungsten wire were simulated, without regard to quantum statistics. The wire was simulated to run in the direction from the chestwall towards the nipple. For simplicity, a single plane orthogonal to the wire was considered – that closest to the chestwall. This simplification allowed us to consider a parallel beam geometry as the simultaneous scanning of the detector and x-ray tube provides for this geometry in the scanning direction.

Image reconstruction was performed by simple backprojection, as is performed in the current prototype. The simulation was implemented in Matlab (Version 6.5.1, Mathsoft, Natick, MA). In addition to producing images, the modulation transfer function (MTF) was calculated in a line orthogonal to the camera that passes vertically through the wire by treating the vertical trace through the wire as the impulse response. The Fourier transform of the impulse response was calculated and normalized to unity at zero spatial frequency to calculate the MTF. The vertical MTF is useful as it provides a measure of the out-of-plane resolution of the tomosynthetic images produced

2.2. Rabbit Simulation

A cadaveric rabbit was imaged using the prototype XC Mammo -3T system described above. 45 projection images were produced over an angular range of 22°, each image differing from the adjacent by 0.5°. The projection images were acquired with 100μm dels at 30 kVp, a W-anode, 0.5 mm Al filtration, and a total dose of 2.5 mGy. The rabbit was approximately 6-8 cm thick, and is comparable in attenuation to a breast of similar thickness.

The projection images of the rabbit were used to simulate the effect of various acquisition geometries. Roughly speaking, tomosynthetic reconstructions were performed with ×1, ×½, ×¼, and ×⅛ the number of projection images, while keeping the total quantum noise constant. The effects of reducing the angular range and reducing the number of projection images were considered. The actual simulation conditions are shown in tables 1 and 2.

A key aspect of this simulation was the need to maintain constant the perceived x-ray quantum noise in each of the reconstructions. As the reconstructions involved between 6 and 45 projection images, the total fluence used to produce the reconstructions would vary 8-fold. The requirement of constant x-ray quantum noise was addressed by estimating the noise in each projection image, and then additively increasing the noise for those reconstructions involving a larger number of projection images. In this way, the level of x-ray quantum noise seen in the reconstructions involving 6 projection images was maintained for all other image reconstructions

The noise for each pixel was estimated by identifying a 9×9 ROI centered on that pixel (appropriately handling the boundaries of the images). For each ROI, a least mean-squares bilinear fit was subtracted from the ROI. An estimate of the variance for pixel (*i,j*) was then made using

$$\sigma_{i,j}^2 = \frac{\sum_{9x9} ROI_{i,j}^2}{9^2 - 3} \ .$$

The denominator has been reduced by three to account for the three degrees of freedom used to estimate the bilinear fit. The local noise estimates were then used to simulate increased quantum noise for each projection image used in a given reconstruction. The intensity of each pixel of the projection image in the simulation is given by

$$I'_{i,j} = I_{i,j} + \sqrt{N}\sigma_{i,j}$$

where *I'* is the processed image, *I* is the original projection image, and *N* is a factor corresponding to the simulation conditions as detailed in tables 1 and 2. The result of this processing is to ensure that each simulated tomosynthesis reconstruction has equal noise.

As with the wire simulation, simple backprojection was used for image reconstruction. Unlike the wire simulation, the reconstruction was performed using software developed at the University of Pennsylvania to produce clinical images from the prototype XC Mammo -3T breast tomosynthesis system. Note, however, that this is not the software used commercially by the manufacturer.

Projections	Angular Range	*N*
6	2.5°	0
12	5.5°	1
23	11°	3
45	22°	7

Table 1: The effect of the angular range was simulated with approximately ×⅛, ×¼, ×½, and ×1 the number of views of the full reconstruction. Noise (of factor *N*) was added to each projection to ensure that the total x-ray quantum noise in each reconstruction was constant.

Projections	Angular Range	*N*
6	22°	0
12	22°	1
23	22°	3
45	22°	7

Table 2: The effect of the number of projection angles was simulated with approximately ×⅛, ×¼, ×½, and ×1 the number of views of the full reconstruction. Noise (of factor *N*) was added to each projection to ensure that the total x-ray quantum noise in each reconstruction was constant.

3. RESULTS

3.1. System Performance

In tomosynthesis, the noise in the reconstructed images will scale with the noise in each of the projection images. In order for the tomosynthesis reconstructions to be dominated by x-ray quantum noise, each projection image must be so dominated. Increasing the number projections used in the tomosynthesis reconstruction will, for the same patient dose, necessarily result in a reduction in the detector dose in each projection. Thus, increasing the number of projections requires that the detector operate with sufficiently little additive noise as to ensure that each projection image is still x-ray quantum noise limited.

To verify the low (or zero) additive noise performance of the prototype x-ray detectors used in this paper, linearity and mean-variance measurements were performed. The image counting time was varied from 0.1 ms to 100 ms in order to alter the total x-ray fluence to the detector. Figure 1 demonstrates the system linearity. A linear regression fit of the data yielded a Pearson correlation coefficient of $R^2 = 1.000$. Figure 2 shows the measured per pixel mean and variance, plotted parametrically as a function of count time; these are the same time points as in figure 1. The figures clearly show that the system is linear and x-ray quantum noise limited to signals as low as 1 photon per pixel; there is no additive detector noise. As a result, the number of angles used in the tomosynthesis reconstruction is not constrained by the detector noise, and tomosynthesis reconstructions using an arbitrary number of angles are possible.

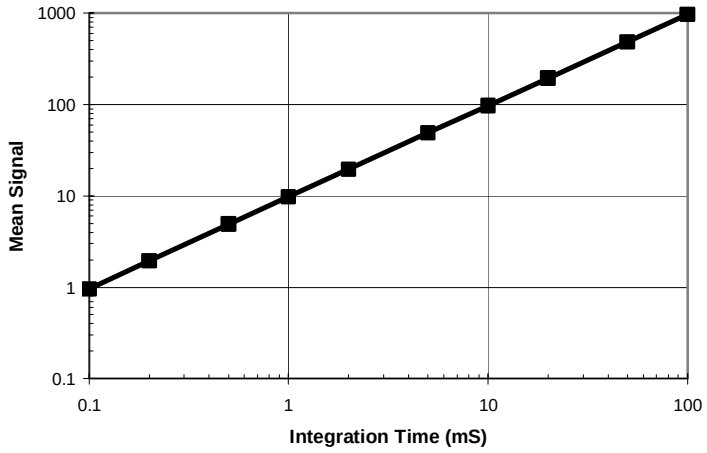

Figure 1: A plot of system linearity. The mean signal is shown as a function of the x-ray exposure integration time. The system is linear over 3 orders of magnitude.

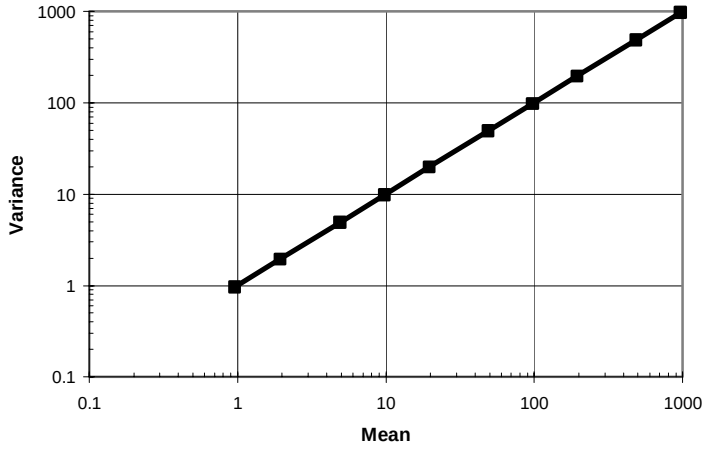

Figure 2: The mean and variance are shown plotted parametrically. These data were measured at various x-ray exposure integration times. The linear relationship between mean and variance is consistent with x-ray quantum-noise limited imaging performance.

3.2. Imaging Simulations

As detailed above, the quality of tomosynthesis image reconstructions is a function of the angular range of the projections, the number of projection angles, and the del size. We performed numerical simulations of imaging a tungsten wire, and we used images of a cadaveric rabbit acquired with the prototype XC Mammo -3T system to simulate variations in the acquisition geometry. We simulated variations of each parameter by performing image reconstructions based on 45, 23, 12 and 6 source images.

3.2.1. Angular Range

The angular range of the reconstructions was varied according to the parameters given in table 1. Effectively, images were produced with ×1, ×½, ×¼, and ×⅛ the full range of projection angles. The simulation of the tungsten wire allowed us to estimate the point-spread function (PSF) of each reconstruction geometry. These data are presented in figure 3. Furthermore, it was possible to estimate the vertical MTF in each instance, as is shown in figure 7 and discussed in section 4.

Examining figure 3, it can be seen that decreasing the range of the projection angles has the effect of increasing the apparent vertical size of the wire. Equivalently, the vertical resolution of the tomosynthetic images is reduced as the angular range is decreased; that is, a given slice will average structures over a greater range of vertical positions. This observation is further supported by the MTF shown in figure 7; as the angular range is reduced, the MTF is also reduced at all spatial frequencies. This observation is discussed further is section 4.

Tomosynthetic images of the rabbit, produced for the various simulated geometries using projection images with appropriately modified noise, are shown in figure 5. The images are shown for three separate regions of the rabbit. The leftmost column is of the thorax, centered on the sternum. The center and rightmost columns show a region of the abdomen (predominantly the stomach and liver). The two columns differ in that the reconstructed slices are separated vertically by 7 mm.

It is noteworthy that the use of 45 projections results in the best image quality. The joints of the sternum, for example, are clearly visualized, while the ribs and other bony and soft tissue structures are effectively removed by blurring. As the angular range of the projection images is reduced, the sternum appears sharper, but this is deceptive as less out-of-plane blurring is occurring; thus more out-of-plane structures are visible, and the resulting images appear more and more like projection radiographs, rather than tomosynthetic reconstructions.

These observations are reinforced when considering the center and right columns of figure 5. These images include the stomach and its contents. Rabbit meal frequently contains crushed calcific material as a nutritional supplement; this is clearly seen as “micro-calcifications” in the images. In the reconstructions based on 45 projection angles, the contents of the stomach are clearly seen, and, for example, the calcifications seen in the two images are clearly unique, even though they are only separated by 7mm vertically. As the angular range is reduced, the out-of-plane blurring is reduced and as a result, the calcifications seen in the two images of the stomach (for a given reconstruction geometry) eventually appear in both images; as such, the benefit of tomosynthesis, namely the production of images which suppress out of plane objects, is lost.

3.2.2. Number of Projection Angles.

The number of projection angles used in the reconstructions was varied according to the parameters given in table 2. Effectively, images were produced with ×1, ×½, ×¼, and ×⅛ the full number of projection angles. In the simulated wire images (figure 4), the vertical resolution does not change; however, when the number of angles is reduced, the projections of the wires separate as they diverge from the center. These are the source of noticeable image artifacts.

Tomosynthetic images of the rabbit, produced for the various simulated geometries using projection images with appropriately modified noise, are shown in figure 6. As before, three separate regions of the rabbit are shown. The leftmost column is of the thorax, centered on the sternum. The center and rightmost columns show a region of the abdomen (predominantly the stomach and liver). The two columns differ in that the reconstructed slices are separated vertically by 7 mm.

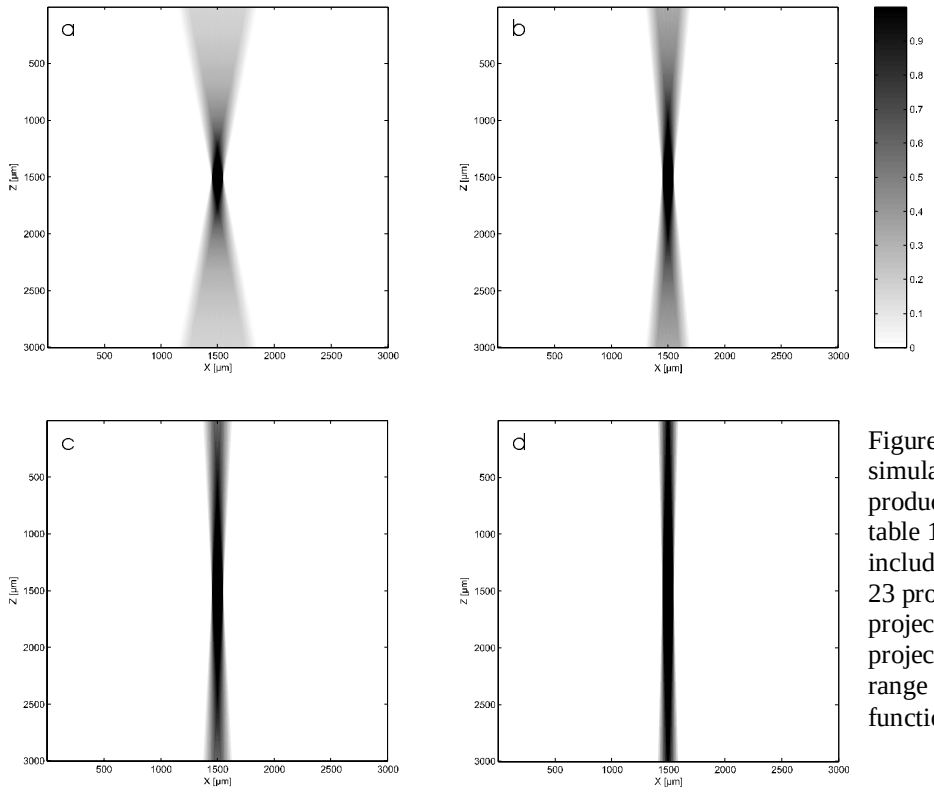

Figure 3: Point spread functions of a simulated 25µm tungsten wire produced for 4 geometries (see table 1) are shown. The geometries include: a) 45 projections over 22°; b) 23 projections over 11°; c) 12 projections over 5.5°; and d) 6 projections over 2.5°. As the angular range is reduced, the point spread function becomes more elongated.

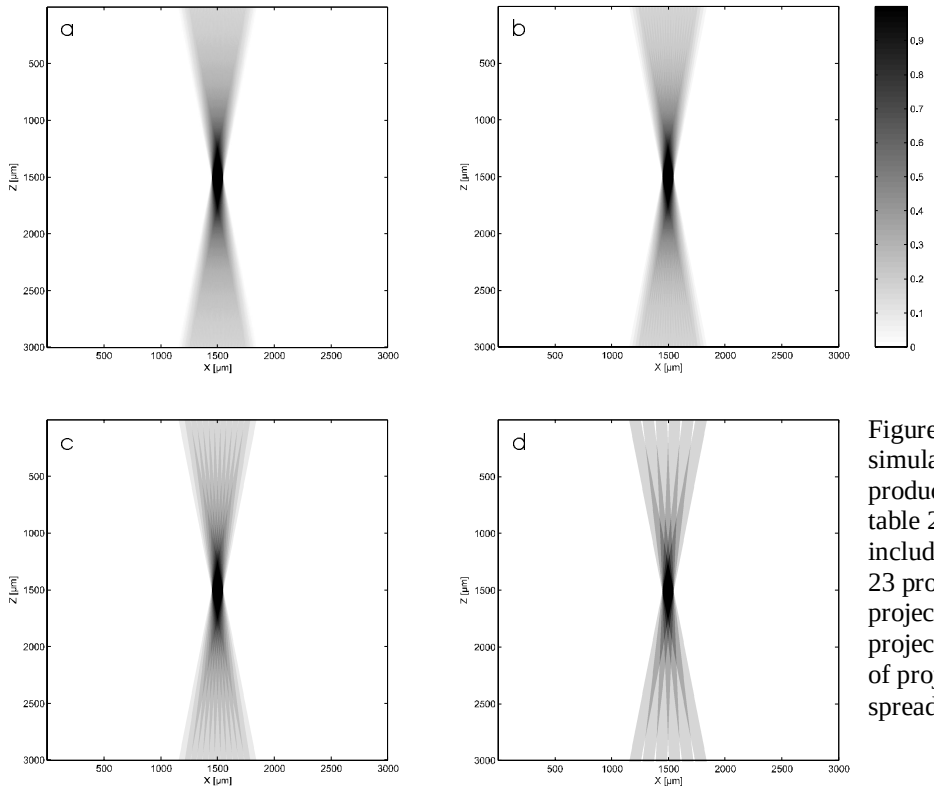

Figure 4: Point spread functions of a simulated 25µm tungsten wire produced for 4 geometries (see table 2) are shown. The geometries include: a) 45 projections over 22°; b) 23 projections over 22°; c) 12 projections over 22°; and d) 6 projections over 22°. As the number of projections is reduced, the point spread function becomes striated.

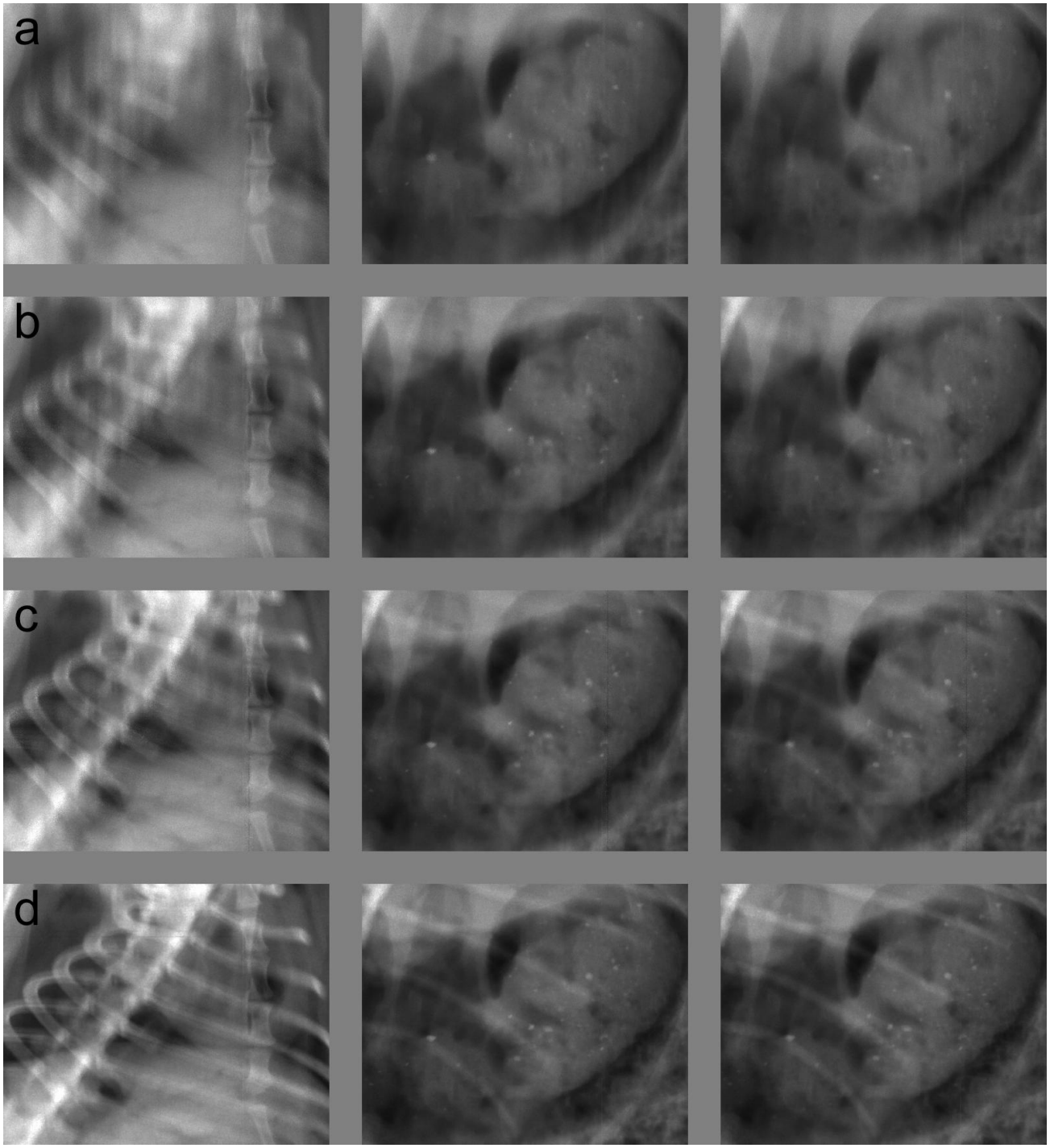

Figure 5: Selected regions of interest from tomosynthetic reconstructions of a cadaveric rabbit. The images were simulated in four different geometries: a) 45 projections over 22°; b) 23 projections over 11°; c) 12 projections over 5.5°; and d) 6 projections over 2.5°. The images were produced with source images modified so that the final reconstructions all have equal perceived noise (see text). The images in the leftmost column are of the thorax, centered on the sternum. The center and rightmost columns are of the stomach and liver. The images in these two columns differ by 7 mm vertically. As the angular range of reconstruction is reduced, the out-of-plane blurring is also reduced.

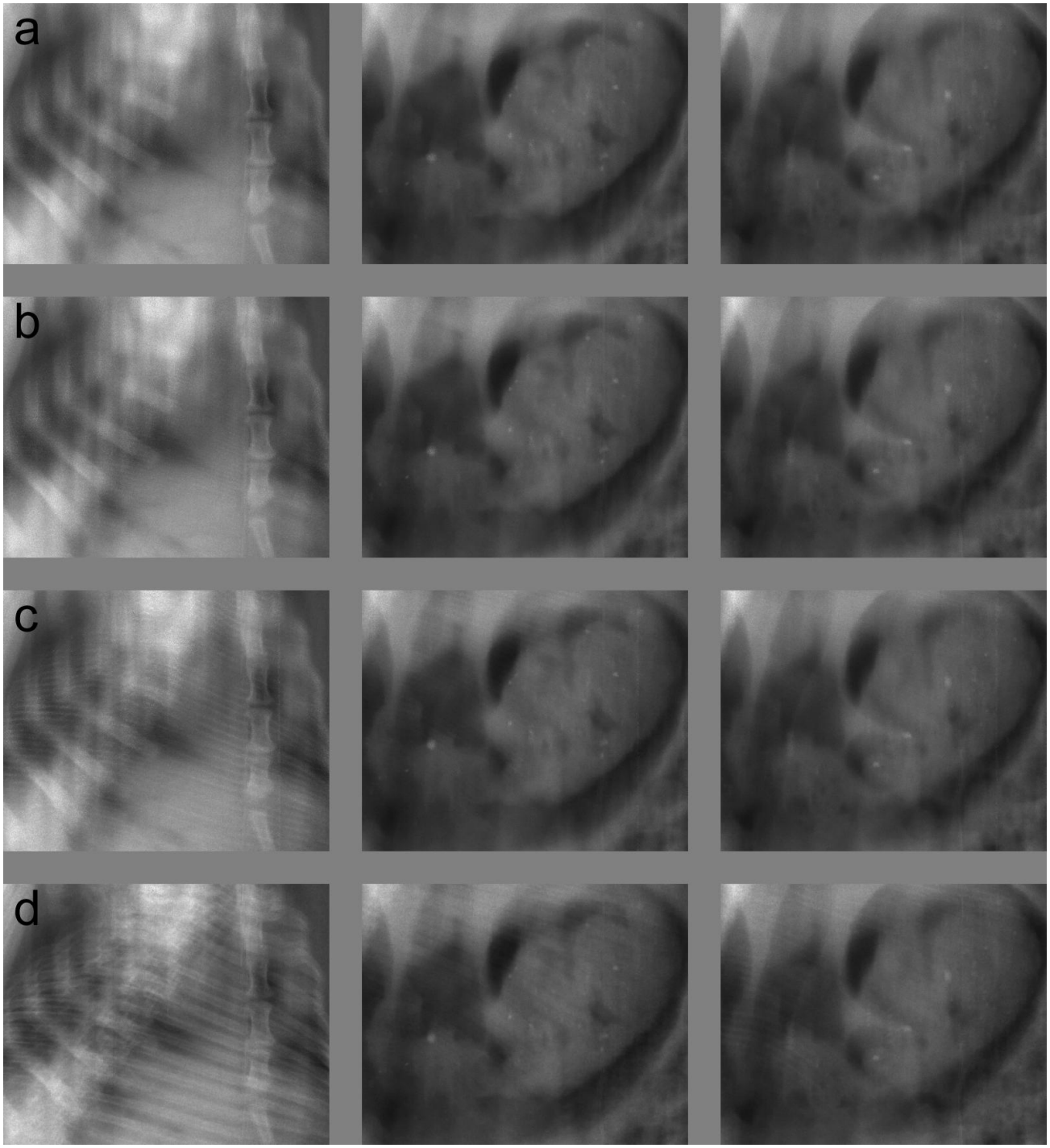

Figure 6: Selected regions of interest from tomosynthetic reconstructions of a cadaveric rabbit. The images were simulated in four different geometries: a) 45 projections over 22°; b) 23 projections over 22°; c) 12 projections over 22°; and d) 6 projections over 22°. The images were produced with source images modified so that the final reconstructions all have equal perceived noise (see text). The images in the leftmost column are of the thorax, centered on the sternum. The center and rightmost columns are of the stomach and liver. The images in these two columns differ by 7 mm vertically. As the number of projections is reduced, reconstruction artifacts become more noticeable.

As in Section 4.2.1, the best image quality is obtained with 45 projections. Reducing the number of unique projection angles (while maintaining the angular range) does not alter the out-of-plane blurring. However, when fewer projections are used in the reconstruction, artifacts due to the reconstruction become increasing obvious. This is not readily evident with 23 projections, although it can be seen in the upper left corner of the rabbit thorax (the left side of the image, rather than left side of the rabbit). With 12 and 6 projections, the artifacts from the ribs and spine become significant.

In the stomach, artifacts are not visible with 23 projections, but are visible with 12 and 6 projections. There are artifacts from the bony structures (ribs and spine), as well as artifacts from out-of-plane calcifications.

4. DISCUSSION

We have attempted to quantify the vertical resolution by calculating a MTF for the various simulated geometries. The long tails in the backprojection reconstruction algorithm produce theoretical difficulties when speaking of a MTF in the vertical direction. Nevertheless, the calculation described has proven to be a useful metric. In figure 7, we show the four different geometries simulated in section 3.2.1, namely: a) 45 projections over 22°; b) 23 projections over 11°; c) 12 projections over 5.5°; and d) 6 projections over 2.5°. We also show, illustratively in the inset figure, how the MTF is calculated using an example produced with 3 projection angles.

It is clear from figure 7, that as the range of angles used in the reconstruction is reduced, the MTF and hence the vertical resolution are similarly reduced. This is as expected; use of a smaller range of projection angles in the tomosynthesis reconstruction will result in less blurring of out of plane structures. It is relevant to note that the limiting MTF for an angular range of 22° is about 0.5 mm^{-1}, or equivalently 1 cycle in 2 mm. This nicely corresponds to the engineering rule-of-thumb that the smallest object resolvable has dimensions of one half the reciprocal of the highest spatial frequency preserved in the signal. We typically reconstruct the tomosynthetic images in 1mm increments. These MTF data provide support for that design choice.

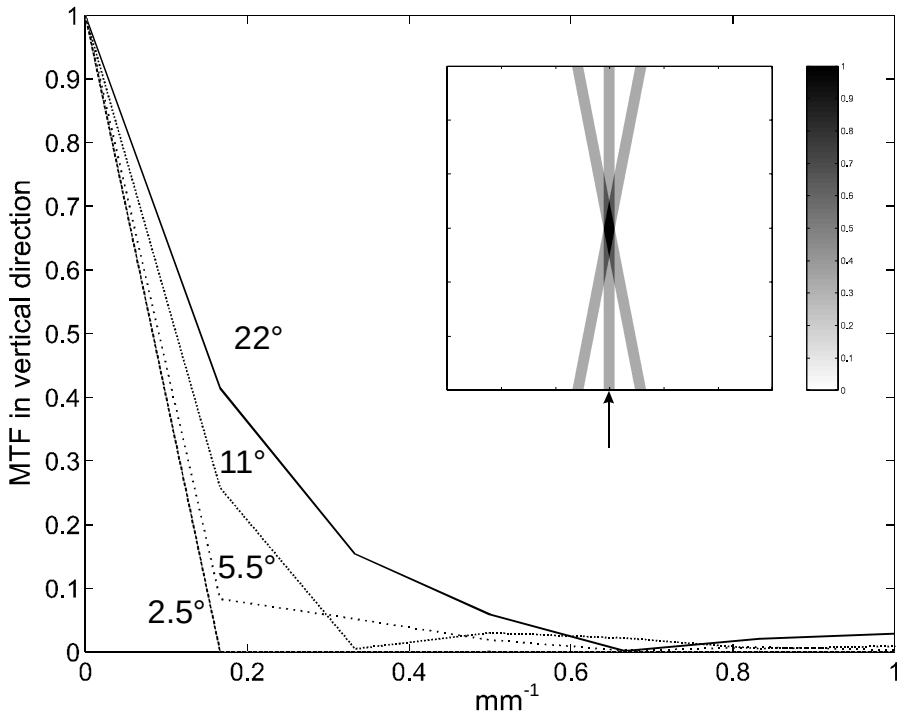

Figure 7: The vertical MTF of four imaging geometries are shown in which the total angular range of the projection images is varied. The geometries are fully specified in table 1. As the angular range is reduced, the MTF is similarly reduced.

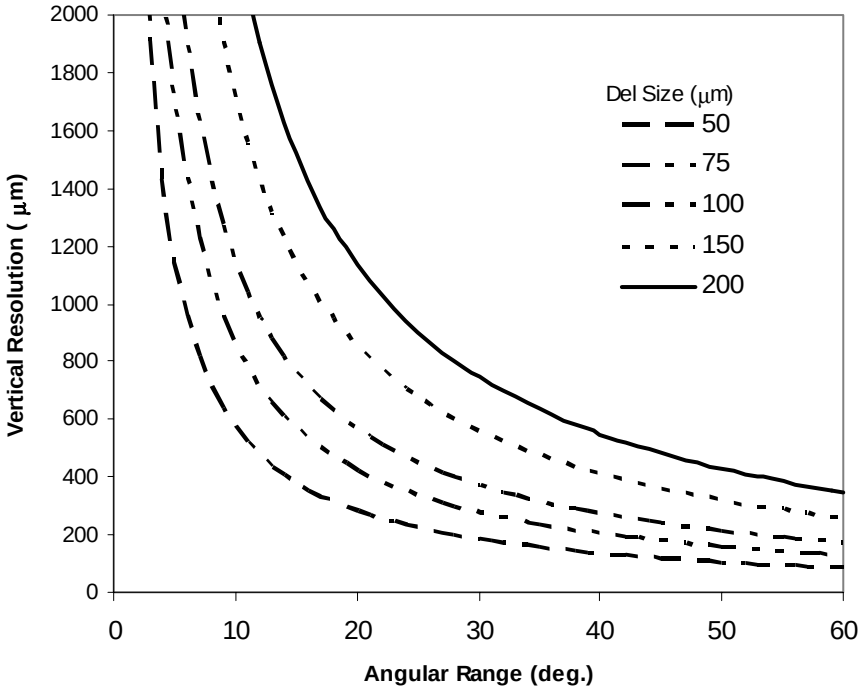

Figure 8: The vertical resolution can be related to the pixel size and the total angular range over which projection images are acquired.

The vertical resolution, Δz, at the limiting frequency can related by

$$\Delta z = \Delta x / \tan(\theta/2) ,$$

where Δx is the del size, and θ is the total angular range of the tomosynthesis projection images. This relationship is shown in figure 8 for a variety of pixel sizes and total angular range.

5. CONCLUSION

Tomosynthesis image quality is a function of many factors, including the number of projection angles, the range of projections angles and the detector element (del) size. We have shown, analytically and through simulations, that both the use of more projection angles and the use of a larger range of projection angles improve the image quality of tomosynthetic image reconstructions. The use of a photon-counting x-ray detector system allows us to consider image acquisition geometries with a large number of projection angles, as there is no additive detector noise to degrade the projection or reconstructed images. The maximum number of projection angles and the range of projections angles do have upper practical limits. The range of projection angles is determined predominantly by the del size. For a 100 μm detector element, that angle is approximately 22°. This is consistent with the XC Mammo -3T x-ray camera design, which uses 45 linear x-ray detectors arrayed over a total of 22°. Further work on this subject is warranted, including consideration of other image reconstruction methods.

REFERENCES

1. L. Ma *et al*., *Case-Control Study of Factors Associated with Failure to Detect Breast Cancer by Mammography,* J. Natl. Cancer Inst., 1992; 84:81-785
2. L. Niklason *et al*. *Digital tomosynthesis in breast imaging*. Radiology 205, 399-406 (1997)
3. J. Dobbins and D. Godfrey, *Digital x-ray tomosynthesis: current state of the art and clinical potential*. Phys. Med. Biol. 48 (2003) R65-R106
4. S. Thunberg *et al*., *Evaluation of a Photon Counting Mammography System,* SPIE Medical Imaging 2002, 4682, 202-208.
5. S. Thunberg *et al*., *Dose reduction in Mammography with Photon Counting Imaging,* SPIE Medical Imaging 2004, 5368, 457-465
6. S. Thunberg , A.D.A. Maidment, *et al. Tomosynthesis with a Multi-line Photon Counting Camera.* Proceedings of the 7th International Workshop on Digital Mammography, In Press (2005).